SBL-BASED JOINT TARGET IMAGING AND DOPPLER FREQUENCY ESTIMATION IN MONOSTATIC MIMO RADAR SYSTEMS

Vini Gupta, Amrita Mishra, Saumya Dwivedi, Aditya K. Jagannatham

Department of Electrical Engineering, Indian Institute of Technology Kanpur, Kanpur, India 208016
e-mail: {vinigupt, amritami, saumyad, adityaj} @iitk.ac.in

ABSTRACT

This paper proposes a novel sparse Bayesian learning (SBL) framework towards target imaging in monostatic MIMO radar systems. Owing to the improved sparse signal recovery guaranteed by SBL, the proposed SBL-based imaging approach is seen to yield a higher resolution and significantly greater sidelobe suppression in comparison to the existing state-of-the-art non-sparse and sparse imaging techniques. Further, a novel joint SBL-based target imaging and angular Doppler frequency estimation scheme is also developed for scenarios with multiple mobile point targets and unknown angular Doppler frequencies. It is demonstrated that the Doppler frequency estimates can be obtained based on a first order Taylor series expansion of the overcomplete dictionary matrix expressed as a function of the Doppler frequencies. Simulation results are presented to validate the efficacy of the proposed techniques.

Index Terms— Monostatic MIMO radar, sparse Bayesian learning (SBL), target imaging, angular Doppler frequency estimation.

1. INTRODUCTION

Active sensing systems such as radars transmit and receive one or more probing signals in order to perform imaging of the potential targets and estimate various target related parameters in the scanning region [1–3]. In this context, a monostatic multiple-input multiple-output (MIMO) radar system employs both transmit and receive arrays with multiple co-located antennas in order to provide improved waveform diversity [4]. However, existing techniques such as delay and sum (DAS), CAPON, iterative adaptive approach (IAA) etc. [5, 6] exhibit poor target imaging accuracy owing to the availability of fewer measurements coupled with the fact that these techniques do not exploit the sparsity inherent in the target distribution.

Recently, several compressive sensing based-techniques have been proposed in the context of target imaging in MIMO radars [7, 8]. Unlike the LASSO-based scheme in [9] wherein one requires tuning of a regularization parameter based on the unknown sparsity level to obtain an approximate sparse solution, other parameter free recovery algorithms, such as sparse learning via iterative minimization (SLIM) [10] and narrowband SLIM-0 [11] etc., do not converge to the maximally sparse solution and thus lead to unwarranted side lobes during the imaging process. In this regard, the sparse Bayesian learning (SBL) framework based on a Gaussian prior, has been utilized for producing the maximally sparse solutions in the context of temporally and spatially sparse MIMO channel estimation [12–14].

Motivated by these observations, this work proposes schemes for point target imaging in monostatic MIMO radar systems based on the SBL framework, considering the scenario wherein both the transmitter and the receiver have only partial knowledge of the Doppler frequencies associated with the targets. Subsequently, a more practical target imaging scenario is considered in which both the MIMO radar transmitter and receiver possess no knowledge of the Doppler frequencies. For this setting, a novel SBL-based scheme is proposed which jointly estimates the reflectivity parameters as well as the associated angular Doppler frequencies of the different targets in the radar scanning range. The proposed technique initially partitions the Doppler scanning region into bins followed by SBL-based estimation of the reflectivity parameters of various targets, employing the perturbed overcomplete dictionary matrix generated using the coarse Doppler frequency estimates. Subsequently, a first order Taylor series approximation of the dictionary matrix, expressed as a function of the Doppler frequencies, is used to obtain the refined angular frequency estimates. Simulation results demonstrate the improved performance of SBL-based imaging in comparison to other non-sparse and sparse schemes for MIMO radar systems.

2. MIMO RADAR SYSTEM MODEL

Consider a narrowband MIMO radar system with M transmit and N receive antennas such that the platform is stationary while the point targets are in motion [10, 15]. Let $\mathbf{x}_i \in \mathbb{C}^{1\times S}$ denote the signal transmitted from the i^{th} transmit antenna. The Doppler shifted signal is, $\mathbf{x}_i(\omega_d) = \mathbf{x}_i \odot \boldsymbol{\phi}(\omega_d) \in \mathbb{C}^{1\times S}$, where $1 \le d \le D$ denotes the d^{th} Doppler bin, ω_d corresponds to the known angular Doppler frequency associated with the target(s) in the d^{th} Doppler bin and the Doppler shift vector $\boldsymbol{\phi}(\omega_d)$ corresponding to ω_d is given by, $\boldsymbol{\phi}(\omega_d) = \left[1, e^{j\omega_d}, \ldots, e^{j\omega_d(S-1)}\right] \in \mathbb{C}^{1\times S}$. The transmit signal matrix $\mathbf{X}_d = \left[\mathbf{x}_1^T(\omega_d), \ldots, \mathbf{x}_M^T(\omega_d)\right]^T \in \mathbb{C}^{M\times S}$ where the transmit steering vector $\mathbf{c}_a = \left[1, \ldots, e^{\frac{-j2\pi d_t (M-1)\sin(\theta_a)}{\lambda}}\right]^T \in \mathbb{C}^{M\times 1}$ and the receive steering vector $\mathbf{d}_a = \left[1, \ldots, e^{\frac{-j2\pi d_r (N-1)\sin(\theta_a)}{\lambda}}\right]^T \in \mathbb{C}^{N\times 1}$ correspond to the a^{th} angular bin $\forall\ 1 \le a \le A$. The quantities d_t, d_r denote the inter-element spacing of the transmit and the receive antenna arrays respectively and θ_a represents the direction-of-arrival (DOA) of the target(s) in the a^{th} angular bin relative to the transmit array. In order to incorporate the maximum possible delay between the reflected signals corresponding to $1 \le r \le R$ range bins, the modified signal matrix can be expressed as, $\widetilde{\mathbf{X}}_d = \left[\mathbf{X}_d \ \ \mathbf{0}_{M\times(R-1)}\right] \in \mathbb{C}^{M\times(S+R-1)}$, where $\mathbf{0}_{M\times(R-1)}$ denotes the $M \times (R-1)$ matrix of zeros. Let $\beta_{r,a,d}$ denote the complex reflectivity parameter proportional to the radar cross section of the point targets present in the r^{th} range, a^{th} angular and d^{th} Doppler bin. The received signal $\mathbf{Y} \in \mathbb{C}^{N\times(S+R-1)}$ can be expressed as,

$$\mathbf{Y} = \sum_{r=1}^{R}\sum_{a=1}^{A}\sum_{d=1}^{D} \beta_{r,a,d}\mathbf{d}_a\mathbf{c}_a^T\widetilde{\mathbf{X}}_d\mathbf{J}_r + \mathbf{Q}, \tag{1}$$

where $\mathbf{Q} \in \mathbb{C}^{N\times(S+R-1)}$ denotes the additive white Gaussian noise matrix and $\mathbf{J}_r \in \mathbb{R}^{(S+R-1)\times(S+R-1)}$ represents the shift matrix used for temporal alignment of the received signals corresponding to different range bins and is given as,

$$\mathbf{J}_r = \begin{bmatrix} \underbrace{0 \quad 0 \quad \cdots \quad 1}_{r} & 0 & \cdots & 0 \\ \vdots & \vdots & \ddots & 1 \\ \mathbf{0} & & & \end{bmatrix}. \tag{2}$$

Using the standard vec operator defined in [16], the vector equivalent $\mathbf{y} \in \mathbb{C}^{N(S+R-1)\times 1}$ of the received signal matrix $\mathbf{Y}$ is given by,

$$\mathbf{y} = \mathbf{\Psi}\mathbf{g} + \mathbf{q}, \tag{3}$$

where the dictionary matrix $\mathbf{\Psi} \in \mathbb{C}^{N(S+R-1)\times RAD}$ is,

$$\mathbf{\Psi} = \left[\boldsymbol{\psi}_{1,1,1}, \boldsymbol{\psi}_{1,1,2}, \ldots, \boldsymbol{\psi}_{R,A,D}\right], \tag{4}$$

with each component $\boldsymbol{\psi}_{r,a,d} \in \mathbb{C}^{N(S+R-1)\times 1}$ given by, $\boldsymbol{\psi}_{r,a,d} = \text{vec}\left(\mathbf{d}_a \mathbf{c}_a^T \widetilde{\mathbf{X}}_d \mathbf{J}_r\right)$ and the weight vector $\mathbf{g} = \left[\beta_{1,1,1}, \ldots, \beta_{R,A,D}\right]^T \in \mathbb{C}^{RAD\times 1}$. Note that each component of the noise vector $\mathbf{q} \in \mathbb{C}^{N(S+R-1)\times 1}$ is independent and identically distributed (IID) with zero mean and variance σ^2. Recent studies [10, 11] have illustrated that owing to the fact that the number of targets present in the scanning region is far less than the total number of potential target locations, the weight vector $\mathbf{g}$ is sparse in nature. Further, the availability of only a limited number of measurements frequently leads to ill-posed estimation scenarios with $N(S+R-1) << RAD$, thus rendering the MIMO radar imaging problem additionally challenging. Existing approaches in literature employ l_1 [9] and l_q [10, 11] norm minimization-based sparse signal recovery techniques in the context of imaging for MIMO radars. However, this work employs the sparse Bayesian learning framework [12] for MIMO radar imaging, owing to its improved performance as exemplified in works such as [13, 14]. Let a parameterized Gaussian prior be assigned to the weight vector $\mathbf{g}$ as, $p(\mathbf{g};\boldsymbol{\gamma}) = \prod_{l=1}^{RAD} (\pi\gamma_l)^{-1} e^{-\frac{|g(l)|^2}{\gamma_l}}$, where $\boldsymbol{\gamma} = [\gamma_1, \gamma_2, \ldots, \gamma_{RAD}]$ such that each γ_l, $0 \le \gamma_l \le 1$, denotes the hyperparameter associated with the l^{th} component of the weight vector $\mathbf{g}$ and corresponds to the reflection coefficient of the l^{th} point target where $l = (r-1)AD + (a-1)D + d$. The next section outlines the proposed SBL-based target imaging technique in the context of MIMO radar systems.

3. SBL-BASED JOINT DOPPLER FREQUENCY ESTIMATION AND TARGET IMAGING

This section initially describes the SBL-based target imaging scheme followed by the development of the proposed joint Doppler frequency estimation and target imaging framework for MIMO radar systems. As illustrated in [12], the iterative expectation maximization (EM) algorithm can be readily employed to obtain the maximum likelihood (ML) estimates $\hat{\boldsymbol{\gamma}}$ of the hyperparameters corresponding to the weight vector $\mathbf{g}$. The expectation (E-step) in the k^{th} iteration evaluates the log-likelihood $\mathcal{L}\left(\boldsymbol{\gamma} \mid \boldsymbol{\gamma}^{(k)}\right) = \mathrm{E}_{\mathbf{g}|\mathbf{y};\boldsymbol{\gamma}^{(k)}}\left\{\log p(\mathbf{y}, \mathbf{g}; \boldsymbol{\gamma})\right\}$ and results in the posterior distribution of the weight vector $\mathbf{g}$ as, $p\left(\mathbf{g} \mid \mathbf{y}; \boldsymbol{\gamma}^{(k)}\right) \sim \mathcal{CN}\left(\boldsymbol{\mu}_g^{(k)}, \mathbf{\Sigma}_g^{(k)}\right)$. The $a\,posteriori$ mean vector $\boldsymbol{\mu}_g^{(k)} \in \mathbb{C}^{RAD\times 1}$ and covariance matrix $\mathbf{\Sigma}_g^{(k)} \in \mathbb{C}^{RAD\times RAD}$ are evaluated as, $\boldsymbol{\mu}_g^{(k)} = \sigma^{-2}\mathbf{\Sigma}_g^{(k)}\mathbf{\Psi}^H\mathbf{y}$ and $\mathbf{\Sigma}_g^{(k)} = \left(\sigma^{-2}\mathbf{\Psi}^H\mathbf{\Psi} + \left(\hat{\mathbf{\Gamma}}^{(k)}\right)^{-1}\right)^{-1}$ where the hyperparameter matrix $\hat{\mathbf{\Gamma}}^{(k)} = \text{diag}\left(\hat{\gamma}_1^{(k)}, \hat{\gamma}_2^{(k)}, \ldots, \hat{\gamma}_{RAD}^{(k)}\right)$. The maximization (M-step) obtains the hyperparameter estimates $\hat{\gamma}_l^{(k+1)}$, $\forall\, 1 \le l \le RAD$ by maximizing the log-likelihood $\mathcal{L}\left(\boldsymbol{\gamma} \mid \boldsymbol{\gamma}^{(k)}\right)$ as [12],

$$\begin{aligned} \hat{\gamma}_l^{(k+1)} &= \arg\max_{\gamma_l \ge 0} \mathrm{E}_{\mathbf{g}|\mathbf{y};\boldsymbol{\gamma}^{(k)}}\left\{p(\mathbf{y} \mid \mathbf{g}; \boldsymbol{\gamma})\right\} + \\ &\quad \arg\max_{\gamma_l \ge 0} \mathrm{E}_{\mathbf{g}|\mathbf{y};\boldsymbol{\gamma}^{(k)}}\left\{p(\mathbf{g}; \boldsymbol{\gamma})\right\} \\ &= \mathrm{E}_{\mathbf{g}|\mathbf{y};\boldsymbol{\gamma}^{(k)}}\left[g(l)^2\right] = \mathbf{\Sigma}_g^{(k)}(l,l) + \left|\boldsymbol{\mu}_g^{(k)}(l)\right|^2, \end{aligned}$$

where $\mathbf{\Sigma}_g^{(k)}(l,l)$ and $\boldsymbol{\mu}_g^{(k)}(l)$ denote the (l,l) and l^{th} elements of $\mathbf{\Sigma}_g^{(k)}$ and $\boldsymbol{\mu}_g^{(k)}$ respectively. After $k = K_{EM}$ EM iterations, the final weight vector estimate is given by, $\hat{\mathbf{g}}_{SBL} = \boldsymbol{\mu}_g^{(K_{EM})}$. It is observed that owing to the superior sparse signal recovery capabilitites of the SBL framework, the hyperparameter estimates $\hat{\gamma}_l$ and the weights $\hat{g}_{SBL}(l)$ corresponding to (r,a,d) i.e. the range, angle and Doppler 3-tuple containing no point targets are driven to zero, thereby substantially enhancing the accuracy of radar imaging.

One of the shortcomings associated with the system model in section 2 is the absence of information regarding the exact Doppler frequency $\widetilde{\omega}_d$ associated with the target(s) corresponding to the d^{th} Doppler bin $\forall\, 1 \le d \le D$. This implies that $\widetilde{\omega}_d$ can take any value between the lower and the upper limits of the d^{th} bin, thus necessitating the development of an improved framework for joint Doppler frequency estimation and target imaging. Owing to the fact that the scanning region of the radar is known, the known Doppler range is partitioned into D Doppler bins with $\omega_d, 1 \le d \le D$ corresponding to the angular frequencies of the bin boundaries. Further, the initial estimate of the Doppler frequency vector $\widetilde{\boldsymbol{\omega}}^{(0)} \in \mathbb{R}^{D\times 1}$ corresponding to the D bins is chosen as, $\widetilde{\boldsymbol{\omega}}^{(0)} = [\omega_1, \omega_2, \ldots, \omega_D]^T$.

For the proposed joint Doppler frequency estimation and target imaging scheme, since the exact Doppler frequency vector $\widetilde{\boldsymbol{\omega}}$ is unknown at the receiver, the dictionary matrix $\mathbf{\Psi}$ for estimation of the weight vector $\mathbf{g}$ using SBL is constructed as per (4) employing the initial Doppler frequency estimates $\widetilde{\boldsymbol{\omega}}^{(0)}$. The weight vector $\hat{\mathbf{g}}_{SBL}$ is estimated using the SBL framework described earlier, followed by segregation of the hyperparameter estimates $\hat{\boldsymbol{\gamma}}$ corresponding to each of the D Doppler bins. Subsequently, the average of the hyperparameter estimates $\hat{\gamma}_{d,avg}$ corresponding to each d^{th} bin is evaluated and this value is compared with a threshold η_{th} chosen heuristically. Corresponding to the Doppler bins $1 \le d \le D : \hat{\gamma}_{d,avg} \le \eta_{th}$, the weight coefficients $\hat{g}_{SBL}(l)$ of the targets of the respective (r,a,d) bins $\forall\, 1 \le r \le R, 1 \le a \le A$ are set to zero. This operation is performed owing to the fact that the Doppler bin(s) corresponding to the target(s) will have a significantly higher value of $\hat{\gamma}_{d,avg}$ unlike the remaining bins where $\hat{\gamma}_{d,avg}$ will evaluate to values close to zero. This further eliminates the necessity to estimate the exact Doppler frequencies corresponding to all such bins where targets are absent. Let a total number of D' Doppler bins satisfy the above criteria and $\Delta\boldsymbol{\omega} \in \mathbb{R}^{D'\times 1}$ denote the difference between the initial and the true Doppler frequency vectors $\widetilde{\boldsymbol{\omega}}^{(0)}$ and $\widetilde{\boldsymbol{\omega}}$ respectively. Note that since the insignificant Doppler bins have been eliminated, $\widetilde{\boldsymbol{\omega}}^{(0)}$ now comprises of the frequencies of the bin boundaries corresponding to only the significant D' bins. Since the dictionary matrix $\mathbf{\Psi}$ can be expressed as a function of the Doppler frequency vector $\widetilde{\boldsymbol{\omega}}$, employing the Taylor series expansion, the true dictionary matrix $\mathbf{\Psi}(\widetilde{\boldsymbol{\omega}})$ can be expressed around the local neighborhood of the initial estimate of the Doppler frequency vector $\widetilde{\boldsymbol{\omega}}^{(0)}$ as,

$$\begin{aligned} \mathbf{\Psi}(\widetilde{\boldsymbol{\omega}}) &= \mathbf{\Psi}\left(\widetilde{\boldsymbol{\omega}}^{(0)} + \Delta\boldsymbol{\omega}\right) \\ &\approx \mathbf{\Psi}\left(\widetilde{\boldsymbol{\omega}}^{(0)}\right) + \frac{\partial}{\partial\widetilde{\boldsymbol{\omega}}}\mathbf{\Psi}(\widetilde{\boldsymbol{\omega}})\Big|_{\widetilde{\boldsymbol{\omega}}=\widetilde{\boldsymbol{\omega}}^{(0)}} \Delta\boldsymbol{\omega}, \end{aligned} \tag{5}$$

where $\Delta\boldsymbol{\omega}$ can be obtained as,

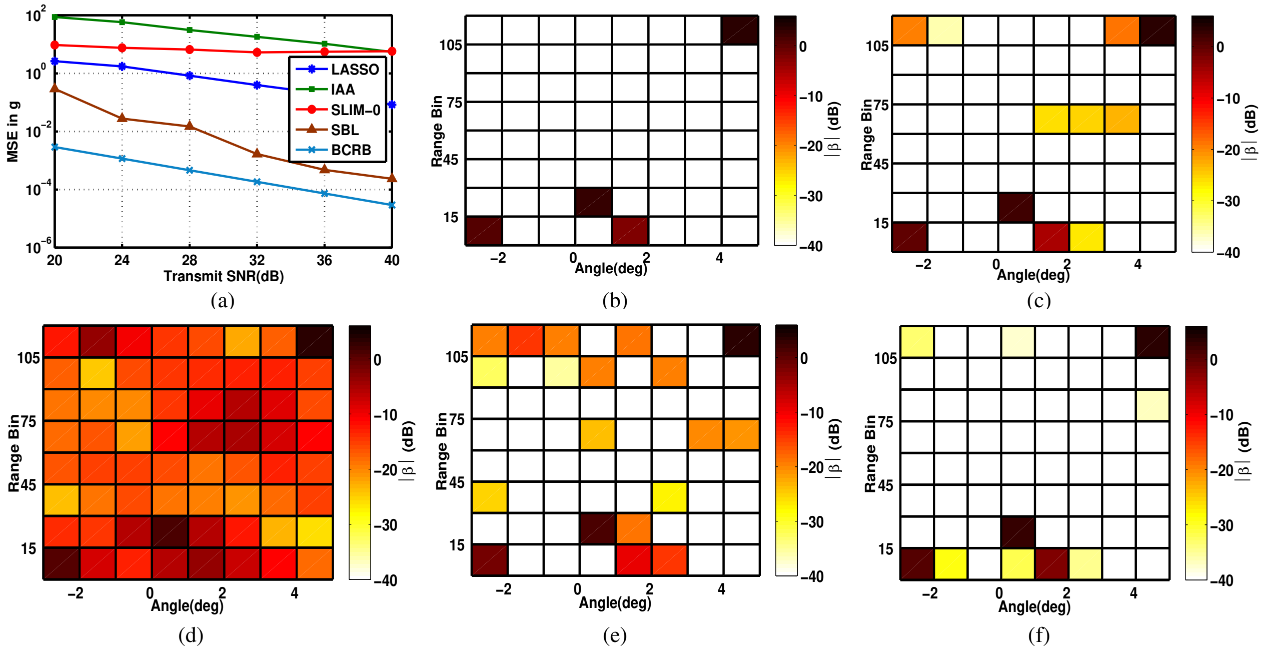

Fig. 1: (a) MSE vs. SNR of weight vector $\mathbf{g}$. MIMO angle-range images for (b) True targets. (c) LASSO estimate. (d) IAA estimate. (e) SLIM-0 estimate. (f) SBL estimate (corresponding to the simulation scenario described in section 4.1).

$$\Delta\boldsymbol{\omega} = \arg\min_{\Delta\boldsymbol{\omega}} \left\| \mathbf{y} - \boldsymbol{\Psi}\left(\widetilde{\boldsymbol{\omega}}^{(0)}\right)\hat{\mathbf{g}} - \left(\frac{\partial}{\partial \widetilde{\boldsymbol{\omega}}} \boldsymbol{\Psi}\left(\widetilde{\boldsymbol{\omega}}\right)\Big|_{\widetilde{\boldsymbol{\omega}} = \widetilde{\boldsymbol{\omega}}^{(0)}} \Delta\boldsymbol{\omega}\right)\hat{\mathbf{g}} \right\|^2$$
$$= \arg\min_{\Delta\boldsymbol{\omega}} \left\| \mathbf{y} - \boldsymbol{\Psi}\left(\widetilde{\boldsymbol{\omega}}^{(0)}\right)\hat{\mathbf{g}} - \mathbf{B}\Delta\boldsymbol{\omega} \right\|^2. \quad (6)$$

The derivative matrix $\mathbf{B} \in \mathbb{C}^{N(S+R-1)\times D'}$ is obtained as, $\mathbf{B} = [\mathbf{b}_j]$, such that each constituent vector $\mathbf{b}_j \in \mathbb{C}^{N(S+R-1)\times 1}$ is given by $\mathbf{b}_j = \frac{\partial}{\partial \widetilde{\omega}_j}\boldsymbol{\Psi}\left(\widetilde{\boldsymbol{\omega}}\right)\big|_{\widetilde{\omega}_j = \widetilde{\omega}_j^{(0)}} \hat{\mathbf{g}}$, $\forall\, j : j \in \mathcal{D}$ where $\mathcal{D}$ denotes the set containing the indices corresponding to the significant Doppler bins and $|\mathcal{D}| = D'$. Further, each component of $\mathbf{b}_j$ evaluates as,

$$b_j\left(N\left(s+r-2\right)+n\right) = \begin{cases} \sum_{i=1}^{M} j\left(s-1\right) x_{i,s}\left(\omega_d\right) e^{-j\frac{2\pi}{\lambda}\sin(\theta_a)[(n-1)d_r+(i-1)d_t]}, \\ \qquad\qquad \forall\, 1 \le s \le S, 1 \le n \le N \\ 0, \text{otherwise} \end{cases}$$

It can now be seen that the solution to the above minimization problem in (6) is obtained as the least-squares solution given by [17], $\Delta\boldsymbol{\omega} = \operatorname{Re}\left\{ \left(\mathbf{B}^H\mathbf{B}\right)^{-1}\mathbf{B}^H\left(\mathbf{y} - \boldsymbol{\Psi}\left(\widetilde{\boldsymbol{\omega}}^{(0)}\right)\hat{\mathbf{g}}\right)\right\}$. Finally, the Doppler frequency vector estimate $\hat{\widetilde{\boldsymbol{\omega}}}$ is obtained as,

$$\hat{\widetilde{\boldsymbol{\omega}}} = \widetilde{\boldsymbol{\omega}}^{(0)} + \Delta\boldsymbol{\omega}. \quad (7)$$

Further, in order to enhance the imaging of point targets, estimation of the SBL-based weight vector $\mathbf{g}$ is repeated using the refined dictionary matrix $\boldsymbol{\Psi}\left(\hat{\widetilde{\boldsymbol{\omega}}}\right)$, constructed employing the estimates of the exact Doppler frequency vector $\hat{\widetilde{\boldsymbol{\omega}}}$ evaluated in (7). Note that the accuracy of the Taylor series approximation in (5) increases as the true Doppler frequencies $\widetilde{\boldsymbol{\omega}}$ associated with the targets in the different Doppler bins lie closer to the bin boundaries. This in turn results in lower perturbation of the dictionary matrix $\boldsymbol{\Psi}$ thereby yielding more accurate Doppler frequency estimates $\hat{\widetilde{\boldsymbol{\omega}}}$.

Table 1: Comparison of simulation results (targetwise Doppler frequency estimate $\hat{\widetilde{\omega}}$ and MSE in $\widetilde{\omega}$) for both regular and finer Doppler grid scenarios

	Case 1:$\Delta\omega_D = 5^o$		Case 2:$\Delta\omega_D = 2^o$	
	$\hat{\widetilde{\omega}}$	MSE	$\hat{\widetilde{\omega}}$	MSE
Target1 ($\widetilde{\omega} = -19.8^o$)	-19.9857^o	0.0345	-19.8572^o	0.0033
Target2 ($\widetilde{\omega} = -13.8^o$)	-15.0022^o	1.4453	-14.1621^o	0.1311
Target3 ($\widetilde{\omega} = -9.8^o$)	-9.9962^o	0.0385	-9.9996^o	0.0398

However, as the exact Doppler frequencies $\widetilde{\boldsymbol{\omega}}$ lie away from the bin boundaries, the associated perturbation in $\boldsymbol{\Psi}$ will increase, thereby yielding inaccurate Doppler frequency estimates. In such a scenario, a natural procedure to obtain robust Doppler frequency estimates is by employing a finer Doppler grid i.e. to increase the number of Doppler bins D by decreasing the angular frequency separation between the adjacent Doppler bins $\Delta\omega_D$. The resulting Doppler frequencies $\widetilde{\boldsymbol{\omega}}$ will now lie closer to the bin boundaries of the refined Doppler bins and the proposed SBL-based joint Doppler frequency estimation and imaging framework described above will yield more precise angular Doppler frequency estimates. Note that, this enhanced performance is however achieved at the cost of increased computational complexity owing to the increase in the number of Doppler bins D for the scenario with a finer Doppler grid.

4. SIMULATION RESULTS

The simulation results below are broadly categorized into two subsections. The first part demonstrates a performance comparison of the proposed SBL-based imaging scheme with other existing techniques, while the second part illustrates the target imaging and mean

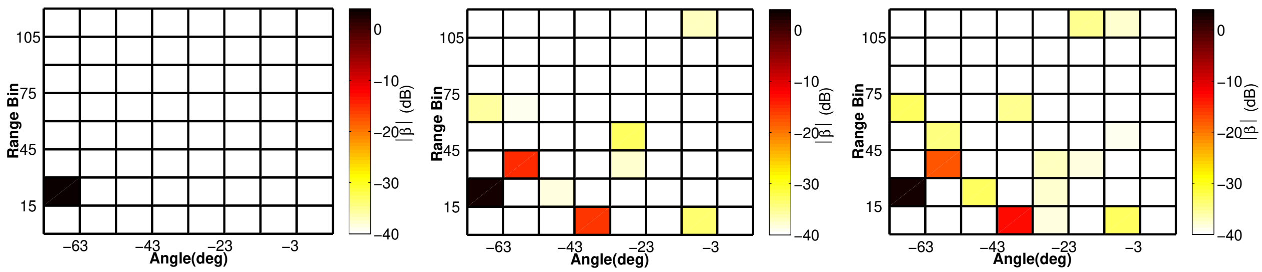

(a) (b) (c)

Fig. 2: MIMO angle-range images for (a) True target. (b) SBL estimate for $\Delta\omega_D = 5^o$. (c) SBL estimate for $\Delta\omega_D = 2^o$.

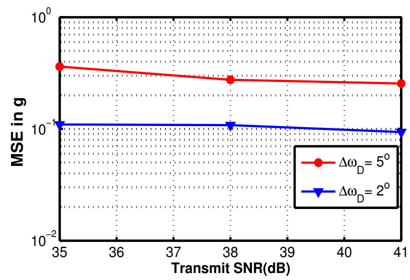

Fig. 3: MSE vs. SNR of weight vector $\mathbf{g}$ (corresponding to the simulation scenario described in section 4.2).

squared error (MSE) performance for the proposed joint Doppler frequency estimation and target imaging technique.

4.1. Performance comparison of SBL versus Existing Imaging Schemes for Monostatic MIMO radar systems

A MIMO radar system with $M = 5$ transmit and $N = 5$ receive antennas, operating at a wavelength of $\lambda = 0.03m$ is considered. The transmit and receive antennas are arranged as uniform linear arrays (ULA) with inter transmit and receive antenna array spacing $d_t = 2.5\lambda$ and $d_r = 0.5\lambda$ respectively [18–20]. Each transmit signal $\mathbf{x}_i$ corresponding to the i^{th} transmit antenna, contains $S = 8$ subpulses of duration $T_s = 0.1\mu s$. The transmit signal to noise power ratio (SNR) is defined as, SNR $= \left(10\log_{10}\left(\text{tr}\left(\mathbf{X}^H\mathbf{X}\right)/S\sigma^2\right)\right)$. Further, a radar imaging scene spanning a range of $0-120$m is divided into $R = 8$ range bins such that the range separation $\Delta R = 15$m, with the angular region ranging from -3^{o} to 4^{o} relative to the array's normal direction with $A = 8$ angular bins such that the separation between the adjacent angular bins is $\Delta\theta_A = 1^{\text{o}}$. The Doppler frequency ranges from -20^{o} to 15^{o} with $D = 8$ Doppler bins which results in separation of $\Delta\omega_D = 5^{\text{o}}$. The Doppler shift $\omega_d(\text{in }^{\text{o}}) = (2\pi f_d T_s)\left(180^{\text{o}}/\pi\right)$ where the Doppler frequency $f_d = 2v_{rel}/\lambda$ and v_{rel} denotes the relative velocity of the radar platform and the target.

The number of targets is set as $P = 8$ and thus the weight vector $\mathbf{g}$ contains 8 non-zero elements. Each reflection coefficient γ_l corresponding to the presence of target in a particular $(r, a, d) : 1 \leq r \leq R, 1 \leq a \leq A, 1 \leq d \leq D$ range-angle-Doppler bin assumes any value $0 < \gamma_l \leq 1$. The maximum number of EM iterations is fixed as, $K_{EM} = 600$ such that the convergence accuracy is $\left\|\gamma_l^{(k+1)} - \gamma_l^{(k)}\right\|_2 < 10^{-3}$. The SBL algorithm is initialized with the hyperparameters $\gamma_l^{(0)} = 1\,\forall\, 1 \leq l \leq RAD$. Fig. 1(a) compares the MSE performance of the reflectivity parameter estimates $\hat{g}(l)$ obtained using various non-sparse and sparse signal recovery techniques such as IAA [6,15], LASSO [9], SLIM-0 [11] and SBL while Figs. 1(b)-(f) depict the angle-range target estimates corresponding to the 6^{th} Doppler bin for various schemes at 32dB SNR. It can be observed that the proposed SBL-based imaging has the lowest MSE in comparison to the existing schemes. Further, Fig. 1(f) shows that the SBL-based approach yields accurate target locations with very low intensity sidelobes thereby demonstrating that it is best suited for target imaging in monostatic MIMO radar systems.

4.2. Joint Doppler frequency estimation and Target Imaging

Consider the same scenario described in section 4.1 with $A = 8$ angular bins which span an angular range from -73^{o} to -3^{o} relative to the array's normal direction with $\Delta\theta_A = 10^{\text{o}}$. The number of targets is set as $P = 3$ with the Doppler frequency vector $\widetilde{\boldsymbol{\omega}} = [-19.8^{\text{o}}, -13.8^{\text{o}}, -9.8^{\text{o}}]^T$. In case 1, the Doppler scanning range $(-20^{\text{o}}$ to $-5^{\text{o}})$ is divided into $D = 4$ bins with separation $\Delta\omega_D = 5^{\text{o}}$ such that $\widetilde{\boldsymbol{\omega}}^{(0)} = [-20^{\text{o}}, -15^{\text{o}}, -10^{\text{o}}, -5^{\text{o}}]^T$. Note that the targets $p = 1, 2,$ and 3 are located each at 4%, 24% and 4% of $\Delta\omega_D$ away from the respective bin boundaries. Further, in case 2, a finer grid is considered for the Doppler range with the Doppler scanning region divided into $D = 8$ bins, $\Delta\omega_D = 2^{\text{o}}$ such that $\widetilde{\boldsymbol{\omega}}^{(0)} = [-20^{\text{o}}, -18^{\text{o}}, ..., -6^{\text{o}}]^T$ and all the targets are now 10% of $\Delta\omega_D$ away from the respective bin boundaries. To maintain a similar convergence accuracy as described previously, the number of EM iterations is chosen as $K_{EM} = 500$ and $K_{EM} = 1100$ for $\Delta\omega_D = 5^{\text{o}}$ and $\Delta\omega_D = 2^{\text{o}}$ respectively. It is observed that after K_{EM} iterations, $\hat{\gamma}_l$ (corresponding to the (r, a, d) 3-tuple containing no point target) lies between $10^{-5} \leq \hat{\gamma}_l \leq 10^{-2}$ which results in $\hat{\gamma}_{d,avg}$ (corresponding to the Doppler bins where targets are absent) $\in \left[10^{-5}, 10^{-2}\right]$. Therefore, η_{th} is fixed as, $\eta_{th} = 10^{-2}$. Table. 1 presents the estimated Doppler frequency $\hat{\widetilde{\boldsymbol{\omega}}}$ at an SNR of 35dB for both the cases. It can be observed that for target 2, the MSE in the estimate of the angular frequency $\widetilde{\omega}$ is lower for case 2 where $\Delta\omega_D = 2^{\text{o}}$. This can be attributed to the fact that the finer grid results in the second target's actual Doppler frequency being closer to the corresponding bin boundary for case 2 when compared to case 1. Hence, the error in $\hat{\widetilde{\omega}}$ corresponding to the second target decreases. Figs. 2(a)-(c) illustrate the SBL-based angle-range images for the second target while Fig. 3 demonstrates that considering a finer grid leads to a reduction in the overall MSE of the reflectivity parameter estimates.

5. CONCLUSION

This paper proposes a SBL-based target imaging framework followed by the development of a novel joint Doppler frequency estimation and target imaging technique in monostatic MIMO radar systems. A comparative simulation study $vis-$à$-vis$ conventional non-sparse and sparse imaging schemes demonstrates the superior imaging accuracy and sidelobe suppression of the proposed SBL-based approach for MIMO radar systems.

6. REFERENCES

[1] M. I. Skolnik, *Introduction to Radar Systems*, McGraw Hill Book Co., New York, 2 edition, 1980.

[2] C. C. Chen and H. C. Andrews, "Target-motion-induced radar imaging," *IEEE Trans. on Aerosp. Electron. Syst.*, vol. AES-16, no. 1, pp. 2–14, 1980.

[3] D. A. Ausherman, A. Kozma, J. L. Walker, H. M. Jones, and E. C. Poggio, "Developments in radar imaging," *IEEE Trans. on Aerosp. Electron. Syst.*, vol. AES-20, no. 4, pp. 363–400, 1984.

[4] J. Li and P. Stoica, "MIMO radar with colocated antennas," *IEEE Signal Process. Mag.*, vol. 24, no. 5, pp. 106–114, 2007.

[5] J. Capon, "High-resolution frequency-wavenumber spectrum analysis," *Proc. IEEE*, vol. 57, no. 8, pp. 1408–1418, 1969.

[6] T. Yardibi, J. Li, and P. Stoica, "Nonparametric and sparse signal representations in array processing via iterative adaptive approaches," in *Proc. of 42nd Asilomar Conf. Signals, Syst. Comput.*, 2008.

[7] R. Baraniuk and P. Steeghs, "Compressive radar imaging," in *Proc. IEEE Radar Conf*, 2007.

[8] L. C. Potter, E. Ertin, J. T. Parker, and M. Cetin, "Sparsity and compressed sensing in radar imaging," *Proc. IEEE*, vol. 98, no. 6, pp. 1006–1020, 2010.

[9] R. Tibshirani, "Regression Shrinkage and Selection via the Lasso," *Journal of the Royal Statistical Society. Series B (Methodological)*, pp. 267–288, 1996.

[10] X. Tan, W. Roberts, J. Li, and P. Stoica, "Sparse learning via iterative minimization with application to MIMO radar imaging," *IEEE Trans. Signal Process.*, vol. 59, no. 3, pp. 1088–1101, 2011.

[11] L. Xu, K. Zhao, J. Li, and P. Stoica, "Wideband source localization using sparse learning via iterative minimization," *Signal Processing*, vol. 93, no. 12, pp. 3504–3514, 2013.

[12] D. P. Wipf and B. D. Rao, "Sparse Bayesian learning for basis selection," *IEEE Trans. Signal Process.*, vol. 52, no. 8, pp. 2153–2164, 2004.

[13] R. Prasad and C. R. Murthy, "Bayesian learning for joint sparse OFDM channel estimation and data detection," in *Proc. of IEEE Global Telecommunications Conference (GLOBECOM)*, 2010.

[14] A. Mishra, A. Pal, A. K. Jagannatham, and K. Rajawat, "Sparse Bayesian learning-based data-aided channel estimation in STTC MIMO systems," in *Proc. of IEEE Australasian Telecommunication Networks and Applications Conference (ATNAC)*, 2014.

[15] W. Roberts, P. Stoica, J. Li, T. Yardibi, and F. A. Sadjadi, "Iterative adaptive approaches to MIMO radar imaging," *IEEE J. Sel. Topics in Signal Process.*, vol. 4, no. 1, pp. 5–20, 2010.

[16] T. K. Moon and W. C. Stirling, *Mathematical methods and algorithms for signal processing*, vol. 1, Prentice hall New York, 2000.

[17] S. Kay, *Fundamentals of statistical processing: Estimation theory*, vol. 1, Prentice Hall America, 1993.

[18] K. W. Forsythe, D. W. Bliss, and G. S. Fawcett, "Multiple-input multiple-output (MIMO) radar: performance issues," in *Proc. of 38th Asilomar Conf. Signals, Syst. Comput.*, 2004.

[19] D. W. Bliss and K. W. Forsythe, "Multiple-input multiple-output (MIMO) radar and imaging: degrees of freedom and resolution," in *Proc. of 37th Asilomar Conf. Signals, Syst. Comput.*, 2003.

[20] J. Li, P. Stoica, L. Xu, and W. Roberts, "On parameter identifiability of MIMO radar," *IEEE Signal Process. Lett.*, vol. 14, no. 12, pp. 968–971, 2007.